Supplementary Information

Integrated and Superaerophilic Ni-O-C Electrode enables Fast and Stable Electrochemical H_2O_2 Production for Electro-Fenton-like Process

Wenwen Xu[1,2,3#], Zheng Liang[4,5#], Shun Gong[1], Baoshan Zhang[1], Hui Wang[1,2], Linfeng Su[1], Xu Chen[1,2], Nana Han[6], Ziqi Tian[1,2], Tanja Kallio[6], Liang Chen[1,2*], Zhiyi Lu[1,2*] and Xiaoming Sun[3]

[1]Institute of New Energy Technology, Ningbo Institute of Materials Technology and Engineering, Chinese Academy of Sciences, 315201 Ningbo, Zhejiang, P.R. China.

[2]University of Chinese Academy of Sciences, Beijing 100049, China

[3]State Key Laboratory of Chemical Resource Engineering, and Beijing Advanced Innovation Centre for Soft Matter Science and Engineering, Beijing University of Chemical Technology, 100029 Beijing, P.R. China.

[4]Frontiers Science Center for Transformative Molecules, School of Chemistry and Chemical Engineering, Shanghai Jiao Tong University, Shanghai, 200240, China

[5]SJTU-Xuchang-Atomic Catalysts & Advanced Materials Joint Laboratory, Shanghai, 200240, China

[6]Department of Chemistry and Materials Science, Aalto University School Chemical Engineering, P.O. Box 16100, FI-00076 AALTO, Finland.

[#]These authors contribute equally. Correspondence and requests for materials should be addressed to L.C (email: chenliang@nimte.ac.cn) and Z.L. (email: luzhiyi@nimte.ac.cn)

Supplementary Note 1

Nernst Equation

The Nernst equation is an equation that relates the reduction potential of an electrochemical reaction (half-cell or full cell reaction) to the standard electrode potential, temperature, and activities (often approximated by concentrations) of the chemical species undergoing reduction and oxidation. Generally, the Nernst equation can be expressed as eq (1):

$$E = E^{\theta} - \frac{RT}{nF} \cdot ln \frac{a_{Red}}{a_{Ox}} \quad (1)$$

where E is the reduction potential, E^{θ} is the standard reduction potential, R is the universal gas constant (8.314 J K^{-1} mol^{-1}), T is the temperature in kelvins, F is the Faraday constant (F = 9.6485×10^4 C mol^{-1}), n is the number of electrons transferred in the reaction, a_{Red} is the activity of the reduced form and a_{Ox} is the activity of the oxidized form.

As for the 2e oxygen reduction in neutral system, the reaction follows the equation (eq (2))

$$O_2 + 2e^- + H_2O \rightarrow H_2O_2 \quad (2)$$

Thus, for this reaction, the Nernst equation can be expressed as eq (3)

$$E = E^{\theta} - \frac{RT}{nF} \cdot ln \frac{a_{H_2O_2}}{p_{O_2}} \quad (3)$$

After the reactant pure oxygen gas was replaced by air, the oxygen partial pressure was reduced to 0.21, which caused a negative potential shift (Δ, eq (4)):

$$\Delta = E_{air} - E_{O_2} = \frac{RT}{2F} \cdot ln \frac{0.21 p_{O_2}}{p_{O_2}} = -0.046\ V \quad (4)$$

Density functional theory calculation: Density Functional theory were performed with the Vienna ab initio simulation package (VASP).[1] The ion-electron interaction was described by employing the projector augmented wave (PAW) method with the Perdew-Burke-Ernzerhof (PBE) functional.[2] The energy cutoff for plan wave was set as 450 eV. The convergence criteria were set to be 10^{-5} eV for energy and 0.03 eV/Å for force. A 5 × 5 × 1 supercell of graphene was employed to build the graphene oxide layer. The vacuum space was 20 Å to avoid artificial interactions between periodic images. The k-points in the Brillouin zone were sampled by a 4 × 4 × 1 grid.

The computational hydrogen electrode (CHE) model[3] was used to calculate the Gibbs reaction free energy change (ΔG) for each step in the two-electron ORR. ΔG value was gained by the Equation S5

$$\triangle G = \triangle E_{DFT} + \triangle E_{zpe} - T\triangle S + eU + \triangle G_{pH} \quad (S5)$$

ΔE_{DFT} is the change of energy. ΔE_{ZPE} and ΔS are the changes of zero point energy and entropy at 298.15 K, respectively. T, e and U are the temperature, the number of transferred electrons and the electrode potential, respectively. ΔG_{pH} is the free energy correction of pH, which can be calculate by the Equation S6：

$$\triangle G_{pH} = k_B T \times \ln 10 \times pH \quad (S6)$$

where the k_B is the Boltzman constant, and pH was set to be zero here. The limiting potential (U_L) is defined as the lowest potential at which all the reaction steps are downhill in free energy.

The total energy (E) and corresponding thermodynamic quantities were listed in Table S2. Since O_2 molecule is poorly described by standard DFT calculations, all the free energies were calculated by using the free energies of H_2O (l) and H_2 (g) as reference.[4,5]The free energies of O_2 molecule and H_2O_2 molecule are determined by equilibrium potential of four-electron (1.23 V vs SHE) and two-electron (0.70 V vs. SHE) ORR, respectively.

For the two-electron ORR, there are two reaction steps[6] (Equation S7 and S8):

$$* + O_2 + H_2O + e^- \rightarrow *OOH + OH^- \quad (S7)$$

$$*OOH + e^- \rightarrow HO_2^- + * \quad (S8)$$

For the hydrogenation of oxygen (equation (1)), ΔG were calculated by following equations:

$$\Delta G_1 = G(*\mathrm{OOH}) - G(*) - G(O_2) - 0.5 * G(H_2) \quad (S9)$$

$$\Delta G_1 = \mathrm{G}(*\mathrm{OOH}) - \mathrm{G}(*) - (4.92 - 2 * \mathrm{G}(H_2) + 2 * \left(G(H_2O)\right) - 0.5 * G(H_2)) \quad \text{(S10)}$$

$$\Delta G_1 = \mathrm{G}(*\mathrm{OOH}) - \mathrm{G}(*) + 4.92 + 1.5 * \mathrm{G}(H_2) + 2 * \left(G(H_2O)\right) \quad \text{(S11)}$$

While for the reduction of OOH* to from H_2O_2 (equation (2)), the ΔG can be obtained directly by Equation S12:

$$\Delta G_2 = -1.4\ eV - \Delta G_1 \quad \text{(S12)}$$

G(*OOH) is defined by the Equation S13:

$$\mathrm{G}(*\mathrm{OOH}) = 4.92 + \Delta G_1\text{-}0.3\ \mathrm{Ev} \quad \text{(S13)}$$

where the empirical solvation correction of -0.3 eV is applied.

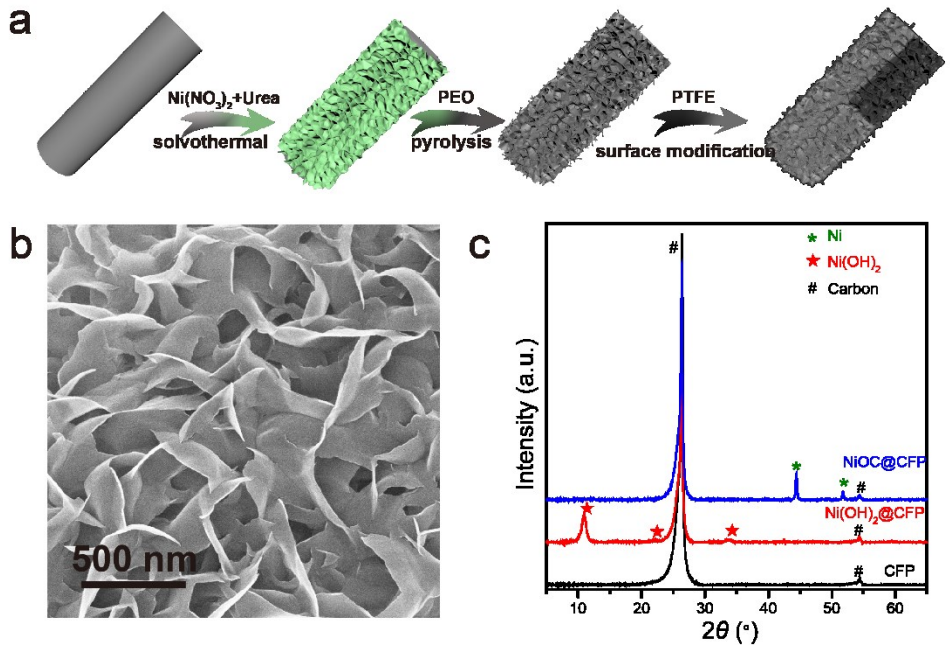

Supplementary Fig.1. (a) Schematic illustration of the IS-NiOC electrode synthesis process; (b) SEM image of $Ni(OH)_2$ array on CFP; (c) XRD patterns of CFP, $Ni(OH)_2$ array on CFP and the NiOC on CFP.

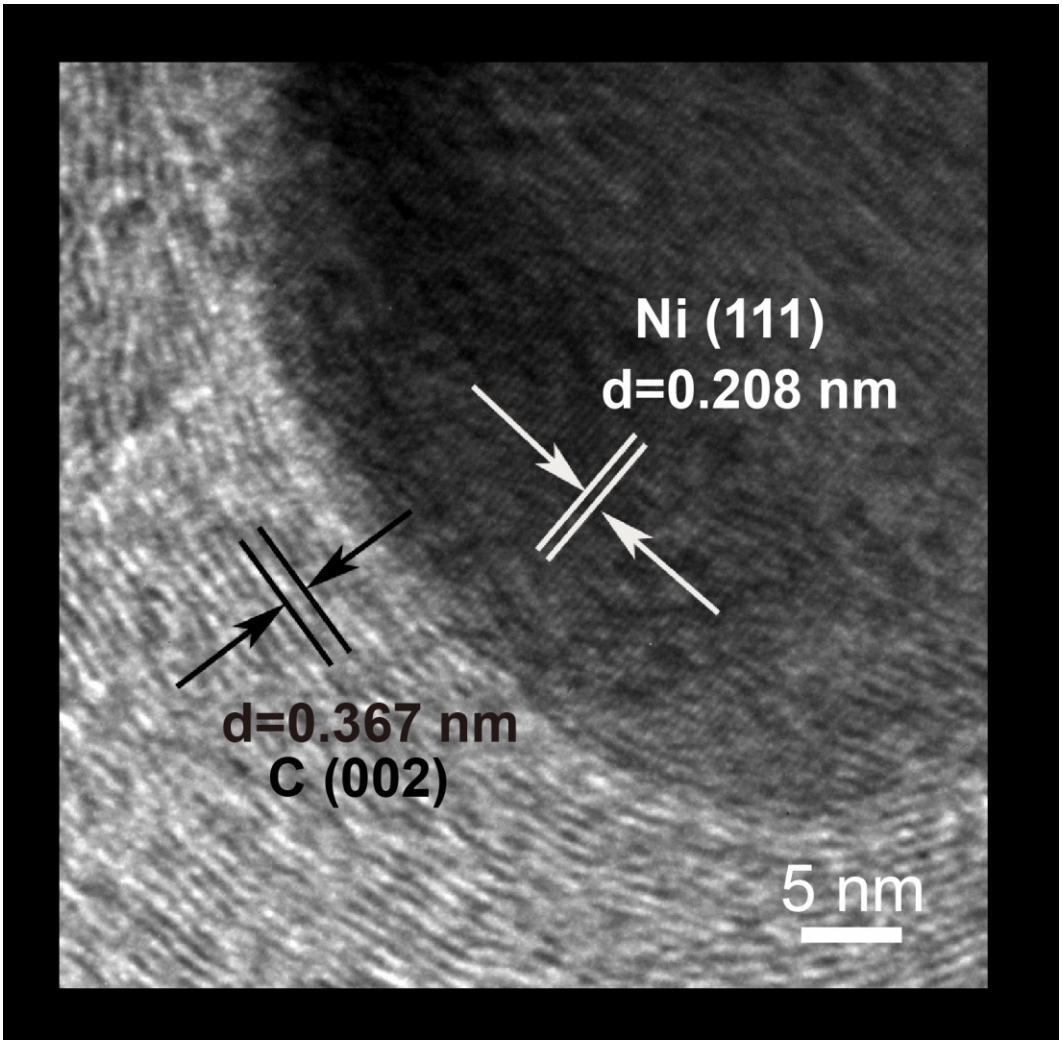

Supplementary Fig. 2. High-resolution TEM image of NiOC illustrated that Ni nanoparticle was encapsulated in the multilayered carbon shell.

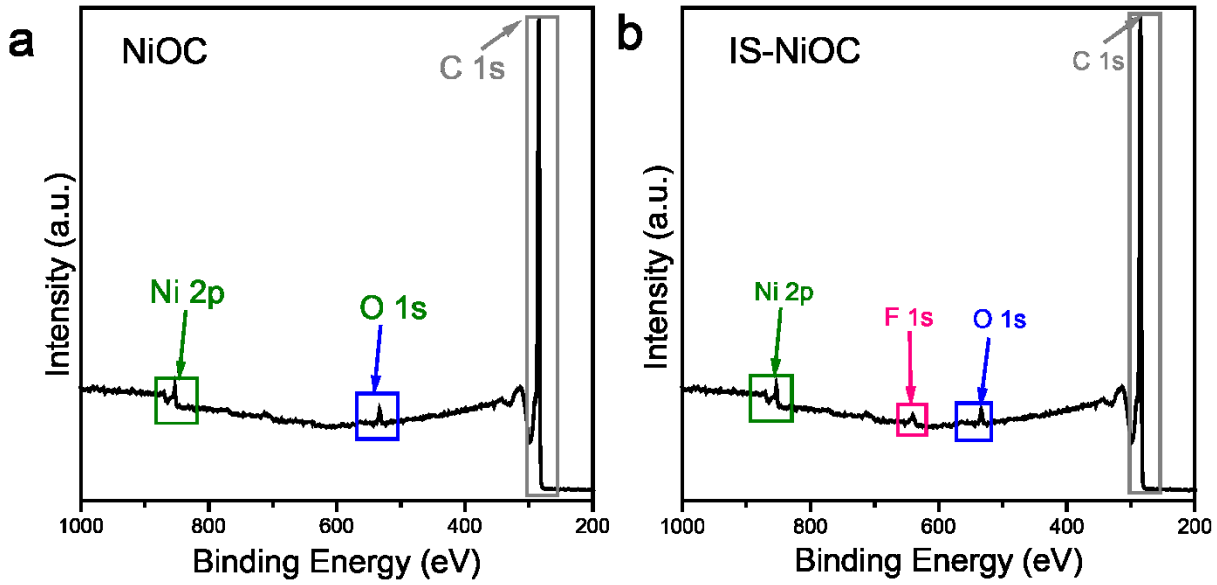

Supplementary Fig. 3. XPS surveys of the (a) NiOC electrode and (b) IS-NiOC. These results indicate that the NiOC electrode was constituted of the Ni, O and C elements, and after the surface modification, the F element was observed.

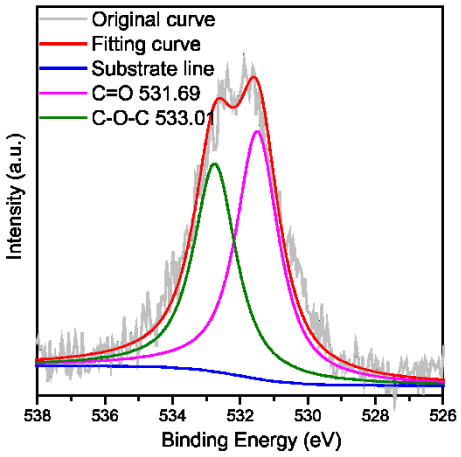

Supplementary Fig. 4. The deconvoluted spectrum of oxygen 1s for oxidized carbon material, only C=O and C-O-C were observed in O-C material.

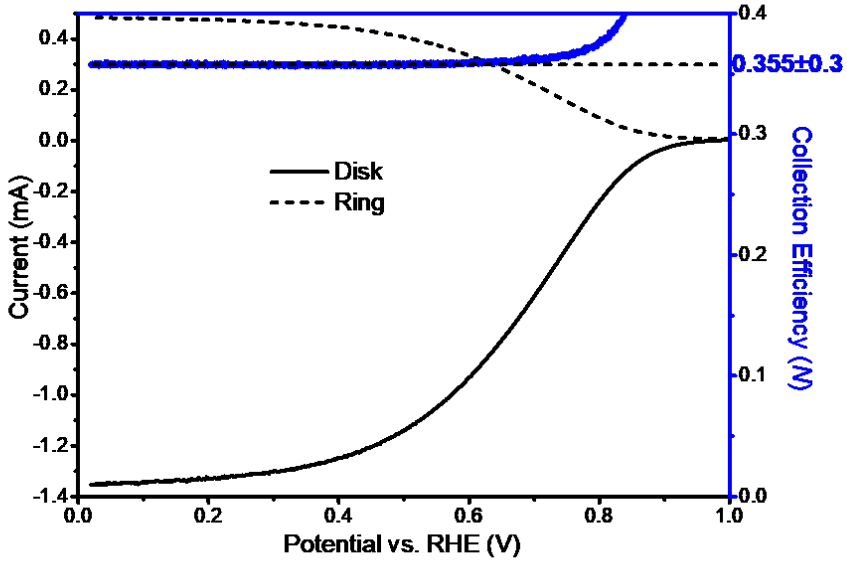

Supplementary Fig. 5. The RRDE collection efficiency was measured by testing the bare glassy carbon rotating disk electrode with Pt ring in N_2 saturated 10mM $K_3[Fe(CN)_6]$ and 0.1M KNO_3 solution. Sweep rates: 10 mv s^{-1}, E_{ring}=1.2 V vs. RHE. The collection efficiency was calculated follow the equation $N=-I_{ring}/I_{disk}$. The experimental determined apparent collection efficiency is ~0.35, close to the theoretical vale of 0.37.

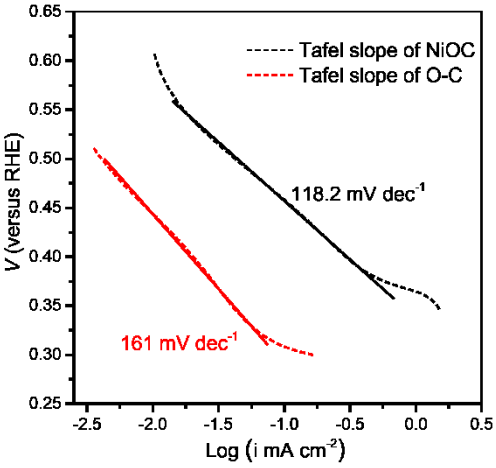

Supplementary Fig. 6. Tafel slopes of NiOC and O-C. The NiOC possessed a much smaller Tafel slope (118.2 mV dec^{-1}) than O-C (161 mV dec^{-1}).

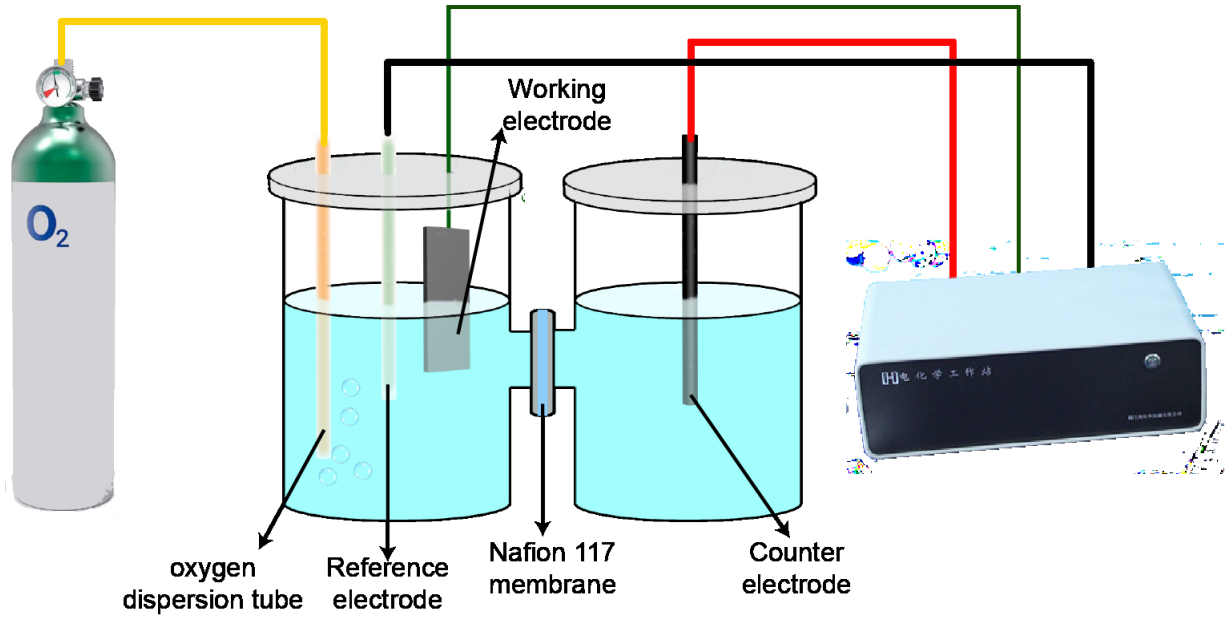

Supplementary Fig. 7. The H-type Cell was established to evaluate the steady ORR performance. The nafion 117 membrane was employed to protect the products on working electrode from decomposed by the counter electrode. The electrolyte was oxygen saturated by continuous bubbling of oxygen.

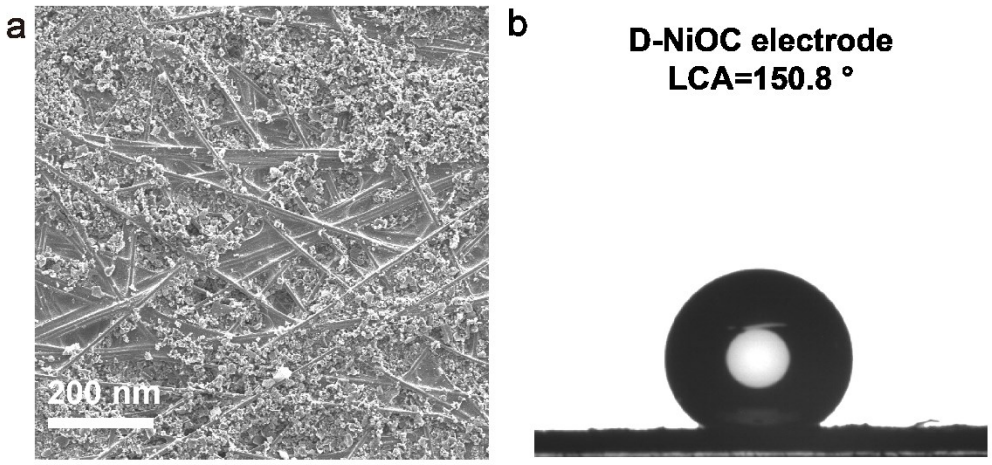

Supplementary Fig. 8. SEM image (a) and LCA (b) of the D-NiOC electrode. Though the D-NiOC electrode possessed a high LCA, no hierarchical architecture was observed, and all the catalysts were loaded on the CFP surface.

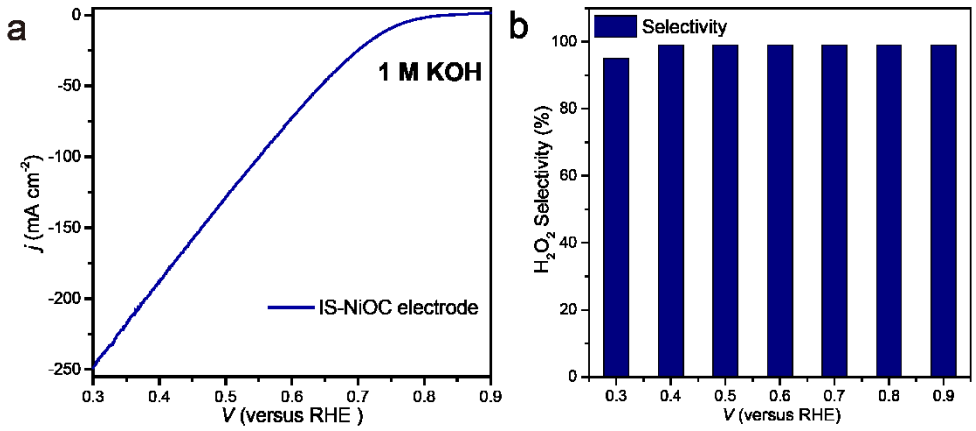

Supplementary Fig. 9. (a) LSV curve (without IR-correction) of IS-NiOC electrode in an H-type Cell with oxygen saturated 1 M KOH solution; (b) corresponding selectivity of IS-NiOC electrode.

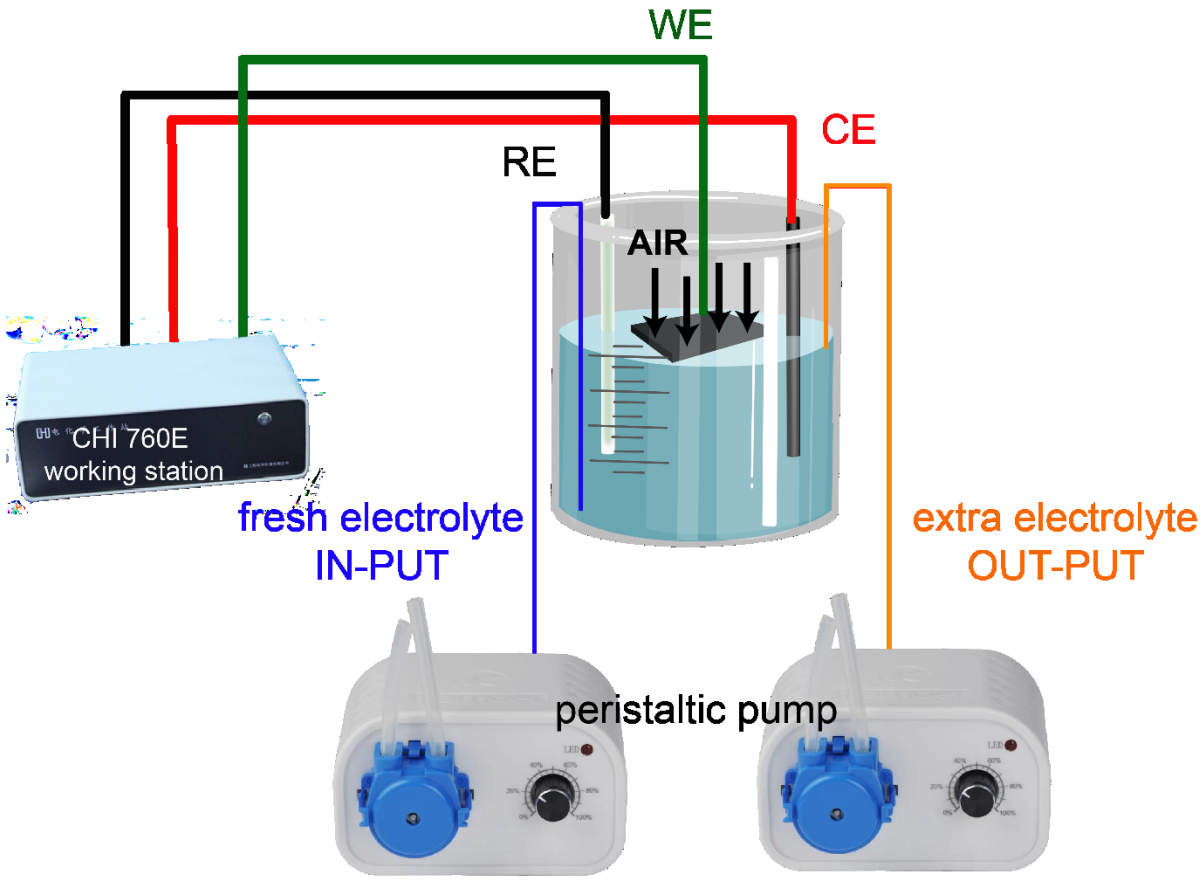

Supplementary Fig. 10. Home-made device was constructed for electrochemical air reduction to produce H_2O_2. The working electrode was floated horizontally on the surface of the electrolyte and the air was absorbed by the up-side surface as the oxygen source. During the long term running, two peristaltic pumps were employed to stabilize the electrolyte level and avoid the H_2O_2 products gathered.

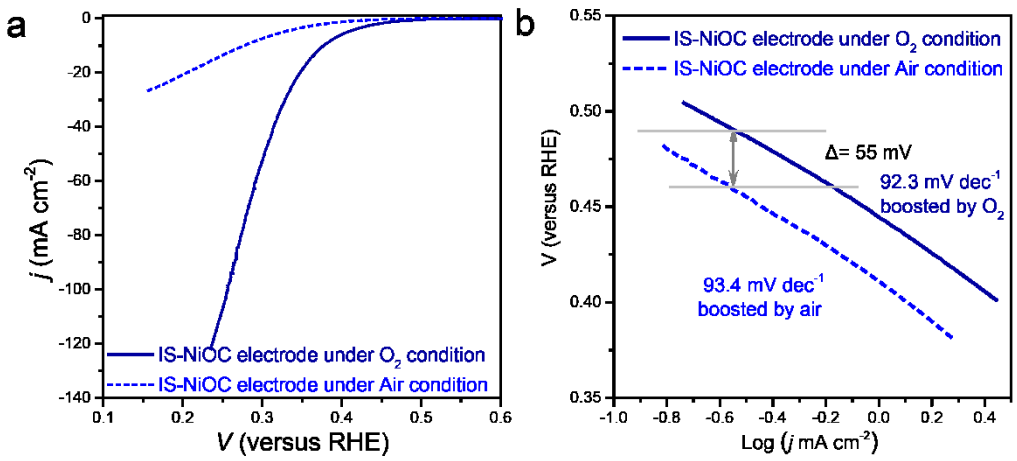

Supplementary Fig. 11. LSV plots (a) and Tafel plots (b) of the IS-NiOC electrode under air and pure oxygen atmosphere, respectively. The IS-NiOC electrode possessed similar Tafel Slopes under air (93.4 mV dec^{-1}) and pure oxygen (92.3 mV dec^{-1}) atmosphere. But an obvious potential shift (55 mV) was observed. According to the Nernst Equation, the concentration fluctuations could directly change the reaction potential. The theoretical value should be 46 mV after the pure oxygen gas was replaced by the air (~21% oxygen).

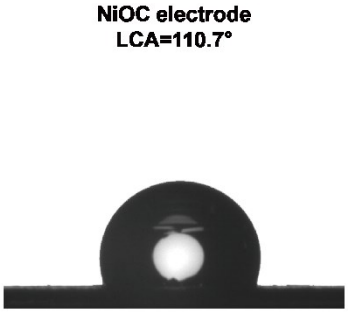

Supplementary Fig. 12. The LCA of the NiOC is 110.7°.

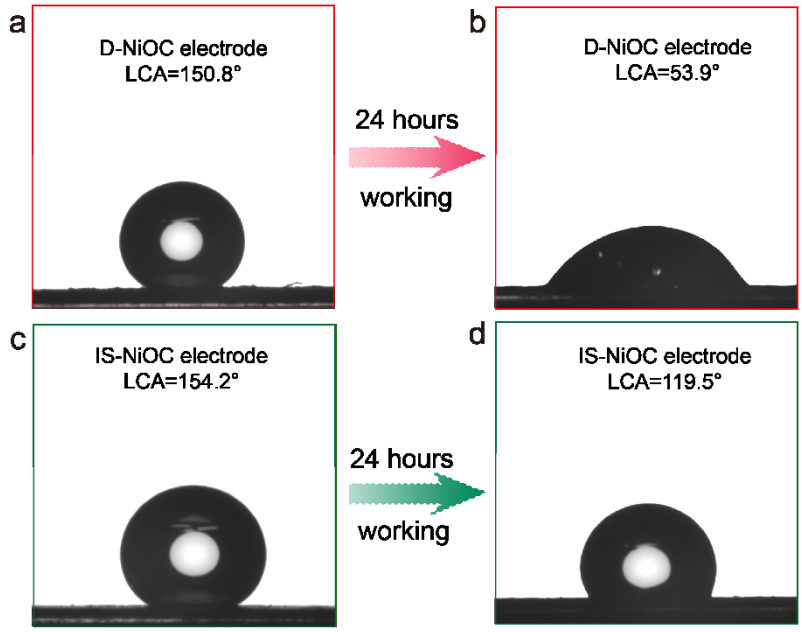

Supplementary Fig. 13. The LCAs of the D-NiOC and IS-NiOC electrode before and after the 24-hours working, respectively. Both the D-NiOC and IS-NiOC electrode suffered from the surface corrosion from the H_2O_2 production. The LCA of the IS-NiOC electrode showed a slight decrease after 24-hours working (ΔLCA=34.7°, from 154.2° to 119.5°). While for the D-NiOC electrode, the LCA exhibited a dramatical drop from 150.8° to 53.9°.

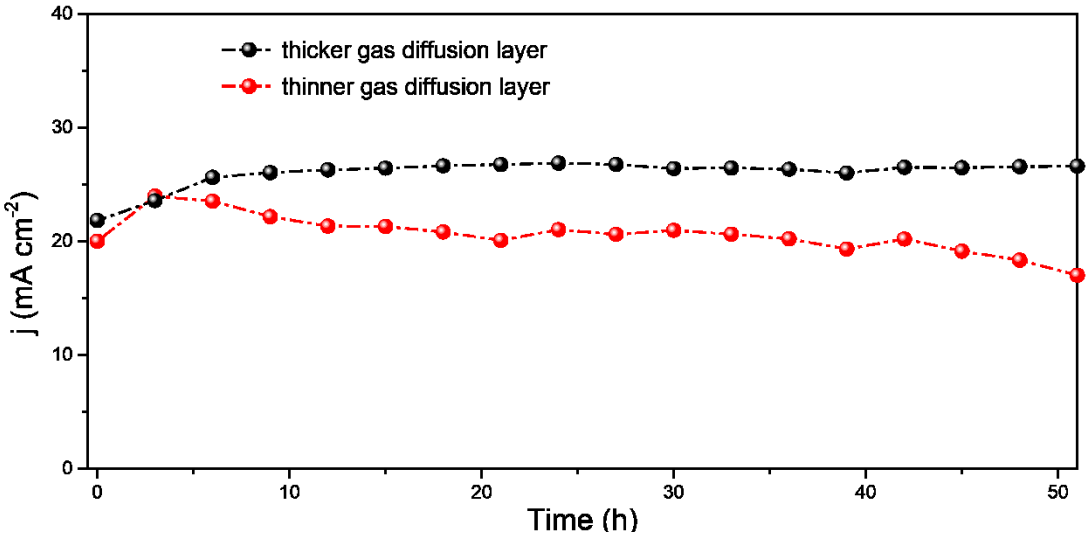

Supplementary Fig. 14. The stabilities of IS-NiOC with different thickness of gas diffusion layers. The IS-NiOC with thicker gas diffusion layer (soaked in 0.1 wt% PTFE for 10 min) performed more stable than the thicker one (soaked in 0.1 wt% PTFE for 8 min) during long-term running. These results confirmed that the diffusion layer can help resistant the oxidation from H_2O_2.

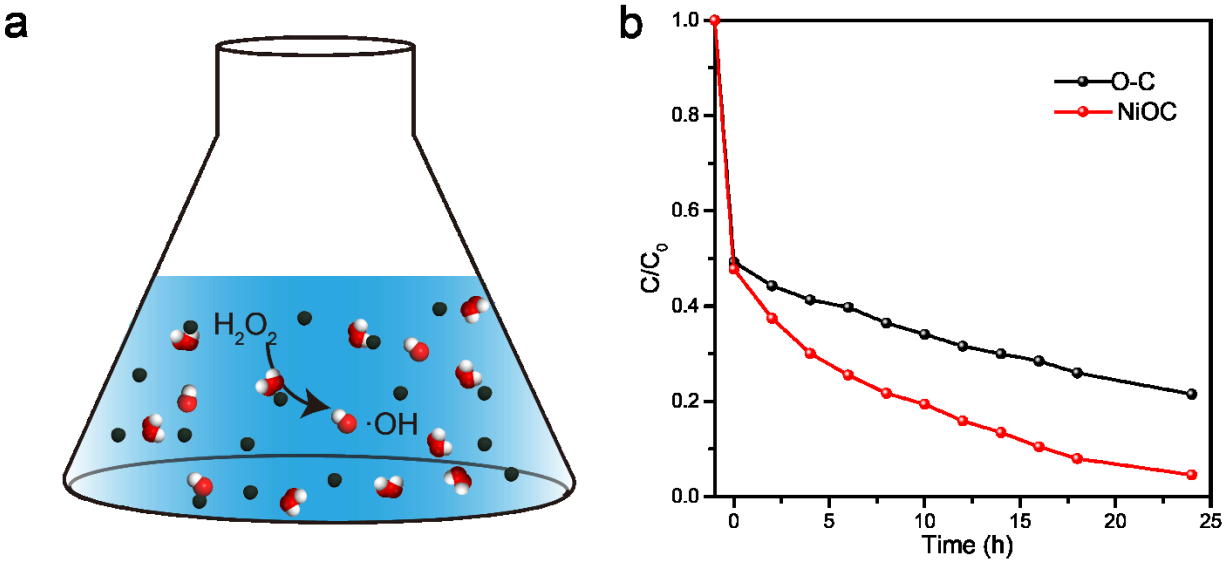

Supplementary Fig. 15. (a) Schematic illustration of Fenton-like reaction system. (b) the NiOC catalyst exhibited a more effective degradability compared with that of O-C catalyst.

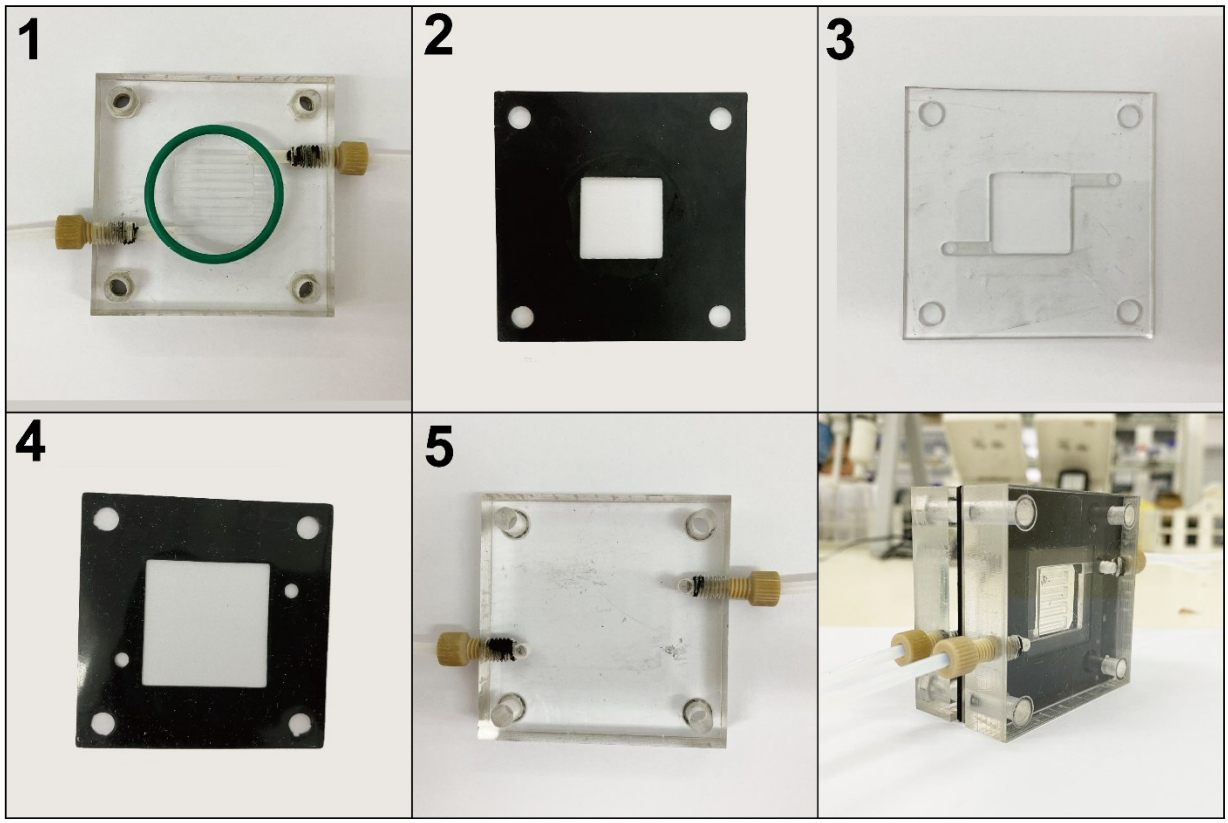

Supplementary Fig. 16. Details of the home-made device for flow state organic degradation.

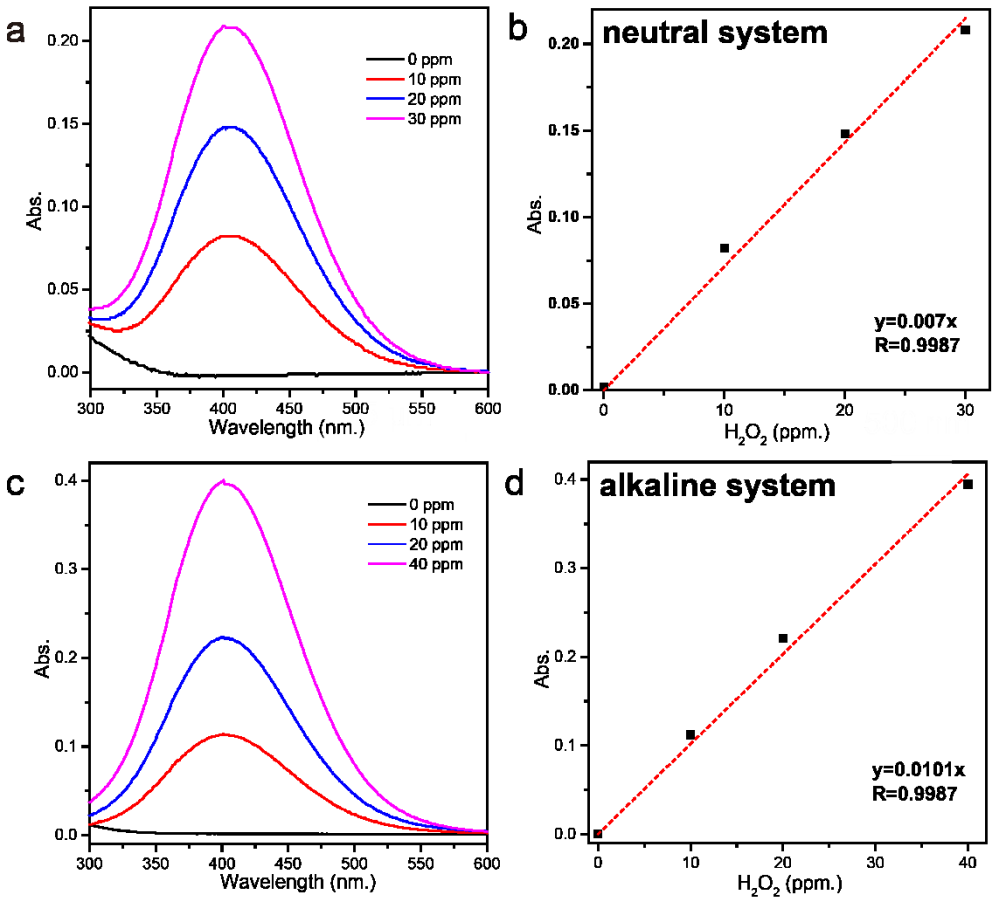

Supplementary Fig. 17. Calibration curves of $Ti(SO_4)_2$ solution with concentrated H_2O_2 in neutral and alkaline medias, respectively.

Supplementary Table 1. Electrochemical ORR results of various reported materials in neutral media.

Catalyst	Electrolyte	H_2O_2 selectivity at 0.2 V (vs RHE)	ref
NiOC	0.1 M PBS	~89%	This work
O-CNTs	0.1 M PBS	82%	[6]
Fe-CNT	0.1 M Na_2SO_4	85%	[4]
g-N-CNTs	0.1 M PBS	51%	[7]

Supplementary Table 2. Calculated total energies and thermodynamic quantities, in eV, for free H_2, H_2O, H_2O_2 species.

Species	E	TS	ZPE	PBE-Correction	G
H_2 (g)	-6.76	0.40	0.27	-0.08	-6.97
H_2O (l)	-14.22	0.67	0.57	-0.06	-14.39
H_2O_2 (l)	-18.16	0.72	0.57	-0.09	-18.28

Supplementary References:

1 Kresse, G. & Furthmüller, J. Efficient iterative schemes for ab initio total-energy calculations using a plane-wave basis set. *Phys. Rev. B* **54**, 11169 (1996).
2 Kresse, G. & Joubert, D. From ultrasoft pseudopotentials to the projector augmented-wave method. *Phys. Rev. B* **59**, 1758 (1999).
3 Nørskov, J. K. *et al.* Origin of the overpotential for oxygen reduction at a fuel-cell cathode. *J. Phys. Chem. B.* **108**, 17886-17892 (2004).
4 Jiang, K. *et al.* Highly selective oxygen reduction to hydrogen peroxide on transition metal single atom coordination. *Nat. Commun.* **10**, 1-11 (2019).
5 Yang, Q. *et al.* Atomically dispersed Lewis acid sites boost 2-electron oxygen reduction activity of carbon-based catalysts. *Nat. Commun.* **11**, 1-10 (2020).
6 Lu, Z. *et al.* High-efficiency oxygen reduction to hydrogen peroxide catalysed by oxidized carbon materials. *Nat. Catal.* **1**, 156 (2018).
7 Iglesias, D. *et al.* N-doped graphitized carbon nanohorns as a forefront electrocatalyst in highly selective O_2 reduction to H_2O_2. *Chem* **4**, 106-123 (2018).